


Article

# Corrosion Prediction Models in the Reinforcement of Concrete Structures of Offshore Wind Farms

Kerman Vázquez \*, Raúl Rubén Rodríguez \* and M. Dolores Esteban \*

Department of Civil Engineering, Universidad Europea de Madrid, 28670 Madrid, Spain

\* Correspondence: kermanvf1994@gmail.com (K.V.); raulruben.rodriguez@universidadeuropea.es (R.R.R.); mariadolores.esteban@universidadeuropea.es (M.D.E.)

**Abstract:** The growth of offshore wind farms (OWF's) is expected to be significant. Reducing operation and maintenance (O&M) costs will be important to ensure its development. The foundation is the most important structural element, with concrete as its main constituent. With concrete structures, particular attention must be paid to corrosion of embedded steel especially in marine environments, as poor maintenance management can have significant economic and structural safety consequences. This article presents a systematic analysis of prevalent corrosion prediction models and the subsequent development of a tool for estimating the diameter loss in the reinforcement of concrete structures in OWFs. For validation, the tool methodology is applied to 32 real cases to evaluate the difference between the calculated and the real diameter loss. The results indicate that the combination between the chloride diffusion model of the Spanish code on structural concrete (EHE-08) and the corrosion rate model of Li (2004) guarantees favourable diameter loss prediction results. The ability to rapidly calculate the diameter loss of reinforcement in concrete structural elements as a function of time, provides OWF operators with a valuable tool for the planning of maintenance strategies and cost optimisation.



**Citation:** Vázquez, K.; Rodríguez, R.R.; Esteban, M.D. Corrosion Prediction Models in the Reinforcement of Concrete Structures of Offshore Wind Farms. *J. Mar. Sci. Eng.* **2022**, *10*, 185. <https://doi.org/10.3390/jmse10020185>

Academic Editor: Carlos Guedes Soares

Received: 22 December 2021

Accepted: 26 January 2022

Published: 29 January 2022

**Publisher's Note:** MDPI stays neutral with regard to jurisdictional claims in published maps and institutional affiliations.



**Copyright:** © 2022 by the authors. Licensee MDPI, Basel, Switzerland. This article is an open access article distributed under the terms and conditions of the Creative Commons Attribution (CC BY) license (<https://creativecommons.org/licenses/by/4.0/>).

**Keywords:** offshore wind; maintenance; foundation; concrete; corrosion; models

## 1. Introduction

Currently, offshore wind installations worldwide have a total installed capacity of 35.3 GW. Europe (UK+27) continues to lead the ranking with 26 GW of installed capacity, which accounts for 70% of global offshore wind installations [1]. China, with 3 GW of installed capacity, has lead offshore installations during 2020, despite the COVID-19 situation [2]. Figure 1 shows the distribution of offshore installations by country in 2020 according to statistics published in [3]. Given the low individual development in some countries, a group called rest of the world (ROW) has been created, which accumulates about 1% of the world's installed offshore wind capacity. This group includes countries such as Spain and Portugal, which only have a few megawatts of installed capacity, with 5 and 25 MW respectively.

To meet the requirements of a climate-neutral energy sector by 2050 and achieve the partial target recently established by the European Union (EU) [4] of reducing greenhouse gas emissions by 55% by 2030, the rate of installations in the wind industry will have to increase significantly in the coming decades. The long-term strategy presented by the European Union in 2018 highlighted the need for 88 GW of installed offshore wind capacity by 2030, and 450 GW (under the maximum scenario) by 2050 in order to reach these targets [5,6]. With the new objectives mentioned above, it necessary to review the 2018 targets and explore options for accelerating the rate of expansion of offshore wind energy. Different references highlight the importance of offshore wind as the alternative technology to achieve decarbonization, as well as the need to industrialize and develop floating offshore wind to drive the energy transition [7]. Exponential growth is forecast for

both technologies in the coming decades, with offshore wind expected to grow to 270 GW worldwide by 2030 and around 16.5 GW to be built globally in the next 10 years.

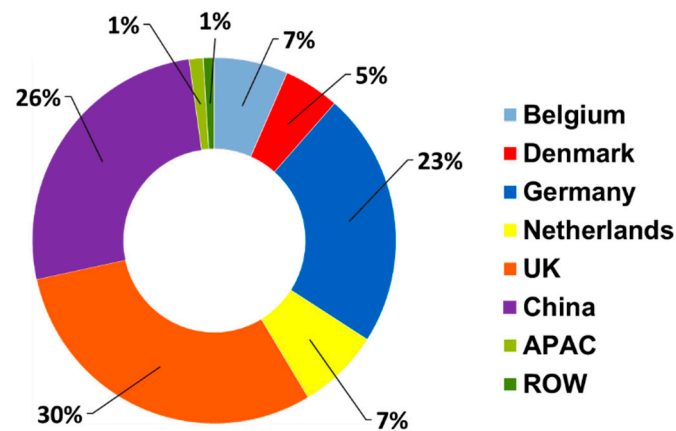


**Figure 1.** Distribution of offshore installations by country in 2020 (Where ROW means rest of the world and it is formed by the following countries: Finland, France, Ireland, Norway, Sweden, Portugal, and Spain).

Achieving this growth entails a number of challenges. In the case of offshore wind, the main obstacle is its high generation cost [8]. One of the elements with the greatest impact on the levelized cost of energy (LCOE) is the wind turbine foundation. The cost of production and installation of the foundation accounts for 25% of the capital expenditure (CAPEX), being together with the turbine one of the most expensive elements among the non-recurring costs of an offshore wind farm (OWF) [9]. Although data on the operation and maintenance (O&M) cost of offshore wind are limited, most references agree that they range between 20 to 30% of the LCOE [10]. No solid references have been found on the maintenance cost of offshore foundations, although some studies estimate that 38% of the operational expenditure (OPEX) is spent on various maintenance tasks, including visual inspections and other activities [11,12].

Currently, in the offshore wind industry there are various types of foundations [13–15]. However, the materials used in these support structures are mainly concrete and steel, sometimes even a combination of both. Although most offshore wind structures and components are made of steel, concrete also has an important role in the offshore wind industry [16]. In Europe, several wind farms have concrete foundations, mostly formed with gravity-based structures [17–19]. Recently, Royal Boskalis Westminster N.V. (Boskalis) in consortium with Bouygues Travaux Publics (Bouygues) and Saipem has been awarded the design, construction, and installation scope for 71 concrete gravity-based structures (GBS) as foundation for the Fécamp OWF in Normandy, France. The development of offshore wind energy in the coming years will require sites located at different distances from shore and water depths to be able to host all offshore wind projects. For this reason, it is expected that opportunities for foundation types such as GBS and others will play a greater role [20]. According to the interactive data tool developed by [21], it is estimated that GBS will remain the second most widely used foundation type between 2026–2030 after steel monopiles, and the importance of concrete in the future of offshore wind support structures is highlighted in [22].

Concrete is also used as the constitutive material of other elements of an offshore foundation, such as the working platform of the transition piece (TP). This type of TP has been used in the foundations of Frysland wind farm (WF), currently under construction, or for the working platform of the TP in West of Duddon Sands WF currently in operation. Going one step further, it is a possibility that, during future development, concrete could be also used in offshore wind turbine towers [23].

The future trend will be towards larger wind turbines and deeper waters, where floating foundations are the best alternative. In the field of floating wind turbines, there are numerous solutions and proposals under development whose main material is concrete, for example the ones mentioned in [24]. Furthermore, now is the time for developed and commercialized innovative floating foundation solutions and other technologies in order to achieve the targets globally set for offshore wind industry [25].

From the above, it can be concluded that concrete is a material that is widely used in the different elements of an OWF, and it seems that it will continue to be useful in the future of the offshore wind industry.

Like any other structure, concrete foundations and elements require periodic maintenance activities to ensure the durability of their materials during their useful life [26]. Particular attention must be paid to this aspect in the case of concrete structures in marine environments, as they face one of their biggest durability problems: corrosion of embedded steel. Corrosion of steel embedded in concrete is an electrochemical process where a flow of electrons from the anode to the cathode occurs through a conductive element (the steel reinforcement) caused by a potential differential [27]. For cathodic reduction to take place, the presence of oxygen and suitable humidity conditions are essential. Fortunately, concrete has a high alkalinity as a result of the products generated during the hydration of the cement [28]. Under these conditions, a passive layer is created around the reinforcement; a microscopic film (free of porosity) of iron oxide and hydroxide residues that protects the steel from corrosion attack [29].

The most common cause of corrosion in steel embedded in concrete located in marine environments is the presence of chloride ions. Chloride ions penetrate the concrete, causing localized breaks in the protective layer. The formation of small anodic zones creates a potential differential, which in the presence of oxygen and humidity conditions initiates the corrosion process [30]. Ultimately, the corrosion process results in a loss of material of the steel bar progressive over time, which causes a loss of strength capacity in the structure. It is therefore crucial to know the evolution of the corrosion of steel embedded in concrete in offshore structures, as this will make it possible to provide the owner of an OWF with a useful data tool for decision-making, managing available resources, and being able to develop different maintenance strategies in order to reduce O&M costs.

In situ tests are now available to determine the corrosion rate in reinforced concrete structures [31], as well as a number of advanced techniques that provide insight into what is happening in embedded reinforcement [32]. These tests and techniques usually require expensive technological equipment or even the need to extract samples of the reinforcement in order to determine parameters such as the corrosion rate in this case, from which the evolution of the diameter loss in the reinforcement can be calculated. The complexity of these activities in the marine environment, the distance from the coast, and the rental cost of equipment for carrying out any type of repair activity on a corrosion-affected element all significantly increase the overall cost of maintenance if they are not properly managed [33,34].

For this purpose, the alternative of corrosion rate calculation models is presented [35], which consists of equations that allow the calculation of the value of the corrosion rate through some parameters of the environmental conditions of the structure and its materials. The characteristics and equations of these models will be developed in more detail in Section 2 of this article. Unlike in situ tests and previous techniques, these models do not require advanced technological equipment, and the work to be carried out to obtain some parameters is simpler and less costly.

The use of mathematical models for the calculation of corrosion rates is not widespread and often generates a feeling of mistrust among technicians specializing in the durability of concrete structures, which often leads to destructive testing and more complex and costly techniques on the structures, and even sometimes not to act on the problem until it reaches a magnitude that puts the safety of the structure at real risk.

This article presents the result of research work where the objective is to develop a tool for calculating the loss of diameter of reinforcement embedded in concrete in foundations or structures of OWF. To this end, existing prediction models for characterizing the useful life (initiation and propagation period) of structures affected by corrosion, which are simple to apply and do not require major actions or extensive testing campaigns on the structure under study, will be applied to a total of 32 real case studies. The results and conclusions will determine the method that best fits reality, whether the use of predictive models is valid or not and reflects reality. It will also allow to know the loss of diameter in a reinforced concrete structure throughout its service life, which is a key aspect for optimizing and programming complex O&M strategies, as well as making better use of the financial and material resources available at this stage in offshore wind installations.

## 2. Materials and Methods

### 2.1. General Methodology

This section describes the methodology used to achieve the objectives of this work (Figure 2). As mentioned above, the development and validation of a tool for calculating the loss of reinforcement diameter in concrete structures, is based on the results and conclusions obtained after applying this work methodology to 32 real case studies, thus the first step was to select the case studies, analyse them, and collect the following data for each of them: general data of the structure, real loss of diameter, parameters that depend on the type of concrete, and parameters that depend on the exposure environment of the structure. All these data will be needed in the following steps.

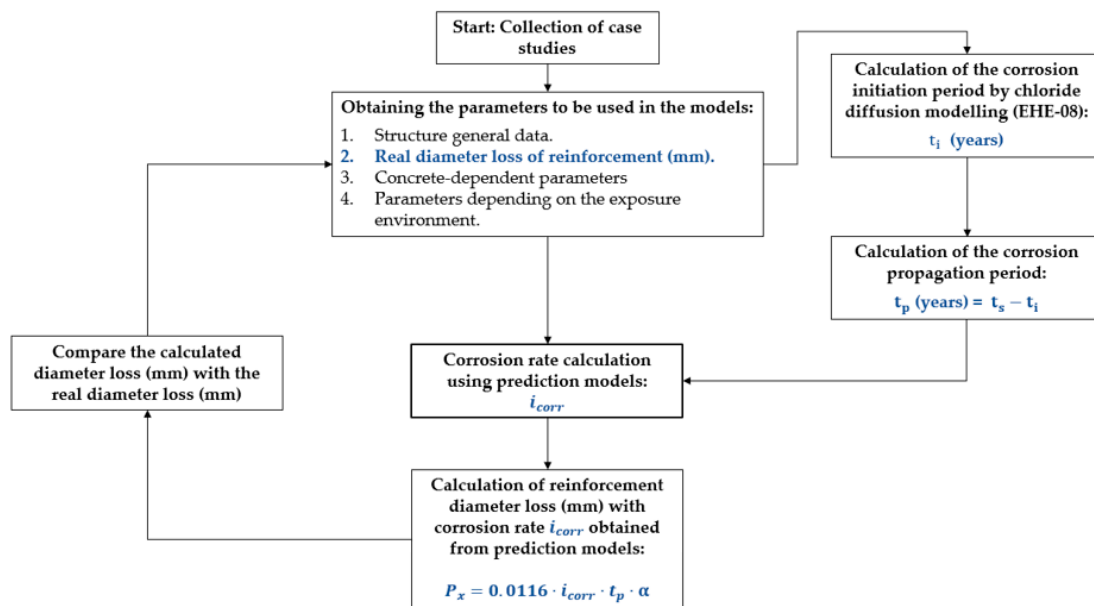
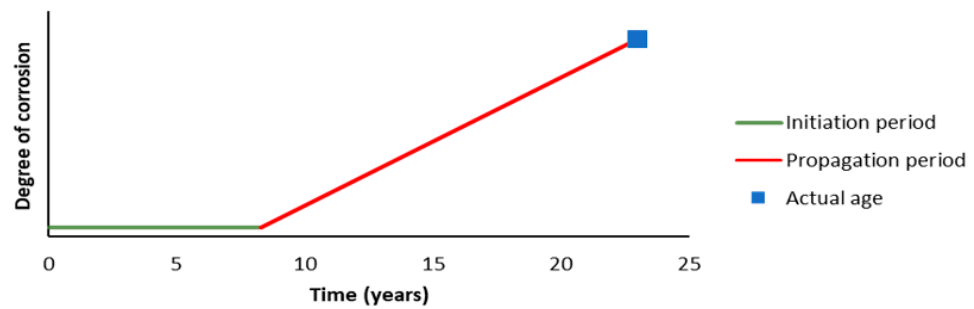


Figure 2. General methodology flowchart to calculate the diameter loss with the proposed corrosion prediction models and validation using real study cases.

The next step is to characterize the corrosion phases. Corrosion of steel reinforcement embedded in concrete consists of two phases: initiation and propagation (Figure 3) [36]. The initiation period is the necessary time for the chlorides, or other aggressive substances, to reach the critical concentration at the reinforcement position and for corrosion to start. Once this threshold is reached, corrosion will start, and the period of the propagation phase will directly depend on the corrosion rate. The sum of both periods estimates the service life of the structure.



**Figure 3.** Qualitative representation of the service life of a structure affected by corrosion (degree of corrosion usually measured in loss of reinforcement section).

Based on the above figure, the first step is to calculate the initiation period ( $t_i$ ). The initiation period is calculated in years, and the simplest and most widely used models are the Fickian diffusion models. Although there are currently several chloride diffusions models as listed in the reference [37], in this case the one proposed by the Spanish code on structural concrete (EHE-08) [38] has been selected. The parameters and equation of this diffusion model are very similar to the one proposed by the International Federation of Structural Concrete (FIB), which is more extended at an international level [39]. The calculation of the initiation period ( $t_i$ ) in the real cases of study will be calculated using Equation (3), for which it will be necessary to know the concrete cover and the chloride concentrations at different depths in each structure.

Once the initiation period has been calculated, the propagation period ( $t_p$ ) is calculated. From the graph in Figure 3, the propagation period can be obtained as the difference between the actual age of the structure ( $t_s$ ) and the corrosion initiation period previously calculated (see Equation (1)). The current years of the structure in service correspond to the moment when a durability study is carried out from which the parameters indicated in the previous point of the flow diagram are extracted. The current age of the structure is obtained from the documentation of each case studied.

$$t_p = t_s - t_i \tag{1}$$

The next step is to calculate the corrosion rate  $i_{corr}$ , which is defined as the rate at which electrons move away from iron in anodic reactions ( $\mu\text{A}/\text{cm}^2$ ) [40] and will therefore determine the rate at which reinforcement will lose diameter over time. The corrosion rate will not remain constant during the propagation period. This is because there are many factors that vary with time and the characteristics of the structure that cause the corrosion rate to be non-constant, especially environmental factors. The main factors are: chloride concentration, humidity, and temperature [41]. It is usually not a simple task to obtain the corrosion rate as on-site measurements are required. This type of work is even more complex on foundations or offshore concrete structures due to the constraints of the marine environment. Fortunately, empirical models have been developed which, using a series of parameters and equations, allow corrosion rates to be calculated more simply. In this work, six existing models (developed in detail in Section 2.2.2) have been analyzed and applied to calculate the corrosion rate using the parameters obtained from each case study (first step in the methodology) and the previously calculated propagation time.

Once the propagation period and the corrosion rate have been calculated for each of the study cases, the diameter loss is calculated using Equation (2) [28].

$$P_x = 0.0116 \cdot i_{corr} \cdot t_p \cdot \alpha \tag{2}$$

where  $P_x$  is the diameter loss (mm), 0.0116 a conversion factor for steel from  $\mu\text{A}/\text{cm}^2$  to mm/year,  $i_{corr}$  is the corrosion rate ( $\mu\text{A}/\text{cm}^2$ ),  $t_p$  is the propagation period (years) and  $\alpha$  is the factor normally adopted for corrosion caused by chloride attack, in this case a

value of 8 is taken as it is the commonly used value [42]. This pitting factor is used to convert a localized section loss due to chloride attack to a generalized section loss of the reinforcement diameter.

Finally, the results of diameter loss in the reinforcement calculated with the corrosion prediction models are compared with the actual diameter loss in the 32 cases studied. The diameter loss data is real and has been obtained in most cases through on-site measurements, which are recorded in the documentation of each of the case studies.

## 2.2. Systematic Analysis of Corrosion Prediction Models

This section presents the systematic analysis that has been carried out on the existing prediction models for estimating the corrosion initiation period and the corrosion rate in reinforced concrete structures.

### 2.2.1. Chloride Diffusion Model

This section presents the equations used for the calculation of the corrosion initiation period using the chloride diffusion model.

In this case, the model proposed by the Spanish code on structural concrete (EHE-08) has been used for the calculation of the corrosion initiation period. The equation of the EHE-08 model is as follows:

$$t_i = \left( \frac{d}{K_{cl}} \right)^2 \quad (3)$$

where  $t_i$  is the initiation period in years,  $d$  is the concrete cover (mm), and  $K_{cl}$  is the chloride penetration coefficient, which is calculated by Equation (4):

$$K_{cl} = \alpha \cdot \sqrt{(12 \cdot D(t)) \cdot \left( 1 - \left( \sqrt{\frac{C_{th} - C_b}{C_s - C_b}} \right) \right)} \quad (4)$$

where  $\alpha$  is a unit conversion factor taken as 56157,  $C_{th}$  is the critical chloride concentration (% weight of cement),  $C_{th}$  critical chloride concentration (% weight of cement),  $C_s$  surface chloride concentration (% weight of cement),  $C_b$  chloride content contributed by the raw materials (aggregates, cement, water, etc.) during manufacture (% weight of cement), and finally  $D(t)$  is the effective chloride diffusion coefficient for age  $t$  calculated by Equation (5) and expressed in ( $\text{cm}^2/\text{s}$ ):

$$D_{(t)} = D(t_0) \cdot \left( \frac{t_0}{t} \right)^n \quad (5)$$

where  $D(t_0)$  chloride diffusion coefficient at age  $t$  whose values have been obtained from the recommendation of the structural code for a reference age  $t_0$  of 28 days ( $t_0 = 0.0767$  years, and  $n$  is the age factor whose value in the absence of tests is assumed to be 0.5.

### 2.2.2. Corrosion Rate Calculation Models

This section presents the equations used for the calculation of the corrosion rate. Existing corrosion rate calculation models have been used to calculate this parameter. After an exhaustive study on the state of the art, this research considers six different prediction models for the calculation of the corrosion rate, listed and developed by reference [35]: (1) Liu and Weyers (1998); (2) Vu and Stewart (2000); (3) Li (2004 a); (4) Li (2004 b); (5) Kong et al. (2006); (6) New Empirical Model (2019).

Liu and Weyers (1998)

This model was carried out in 1998 by creating a database (2927 results) obtained from seven-series specimens exposed to high chloride contamination over a time period of 5 years. The model proposes a non-linear regression which varies with the following

parameters: chloride content, ambient temperature, ohmic strength of concrete, and the duration of the active phase of corrosion (propagation period).

$$i_{corr(t)} = 0.926 \cdot \exp \cdot [7.89 + 0.7771 \cdot \ln \cdot (1.69 \cdot C_t) - \frac{3006}{T} - 0.000116 \cdot R_c] \quad (6)$$

where  $i_{corr(t)}$  is the corrosion rate ( $\mu\text{A}/\text{cm}^2$ ) at time  $t$ ;  $C_t$  is the chloride content at the reinforcement position ( $\text{kg}/\text{m}^3$ ).  $T$  is the temperature in degrees kelvin at the position of the reinforcement;  $R_c$  is the ohmic resistance of concrete (ohms);  $t_p$  is the corrosion propagation time (years).

Regarding the ohmic resistance of concrete, Liu (1996) [43] established a relationship between the ohmic strength of concrete and its chloride content, which has been used to calculate the ohmic resistance of concrete. The equation is as follows:

$$R_c = \exp \cdot [8.03 - 0.54 \cdot \ln \cdot (1 + 1.69 \cdot C_t)] \quad (7)$$

where  $C_t$  is the chloride concentration at the reinforcement position ( $\text{kg}/\text{m}^3$ ) as mentioned above.

Vu and Stewart (2000)

Vu and Stewart (2000) model is focused on structures located in environments with a relative humidity of 75% and an average annual temperature of approximately  $20^\circ\text{C}$ . This model takes into account the water-to-cement ratio ( $w/c$ ) and, unlike the previous model, includes among its variables the concrete cover of the reinforcement. The model is defined by the following equation:

$$i_{corr(t)} = 0.85 \cdot t_p^{-0.29} \cdot i_{corr_0} \quad (8)$$

where  $i_{corr(t)}$  is the corrosion rate ( $\mu\text{A}/\text{cm}^2$ ) at time  $t$ ;  $t_p$  is the propagation period (years) and  $i_{corr_0}$  is the corrosion rate at the beginning of the corrosion propagation period ( $\mu\text{A}/\text{cm}^2$ ). It is calculated as indicated in Equation (9), where  $w/c$  is the water-to-cement ratio and  $d_c$  is the concrete cover depth (mm).

$$i_{corr_0} = \frac{37.8 \cdot (1 - \frac{w}{c})^{-1.64}}{d_c} \quad (9)$$

Bolomey formula shown in Equation (10) has been used to obtain the approximate  $w/c$  ratio, where  $f_{ck}$  is the concrete compressive strength (MPa).

$$\frac{w}{c} = \frac{27}{f_{ck} + 13.5} \quad (10)$$

It is a simple model for application in real cases. However, it is important to note that it does not take into account aspects related to the environment in which the structure is located, neither the relative humidity nor the ambient temperature.

Li (2004 a)

This is the first of the models proposed by Li (2004 a). It is a simple corrosion rate prediction model, easy to apply in real cases, in which the corrosion rate is a function of the duration time of the active phase of corrosion; this is the propagation time ( $t_p$ ).

$$i_{corr} = 0.3683 \cdot \ln(t_p) + 1.1305 \quad (11)$$

As can be seen, this model does not take into account the parameters related to the exposure environment of the structure, nor the physico-chemical characteristics of the concrete, at least not explicitly. However, it does implicitly in this work, since the corrosion

propagation period is obtained using the models proposed by the EHE-08, in which the characteristics of the concrete, such as concrete cover, the age of the structure,  $w/c$  ratio, chloride concentration, and environmental conditions among others are taken into account. This is mainly reflected in Equations (4) and (5).

Li (2004 b)

Following his first model, Li (2004 b) develops another specific model for structures exposed to environments with high chloride concentrations, considering the following parameters: ambient temperature, relative humidity,  $w/c$  ratio, concrete cover, and chloride concentration on the position of the reinforcement. Li (2004 b) proposes the following equation to calculate the corrosion rate:

$$i_{corr}(t) = 2.486 \cdot \left(\frac{RH}{45}\right)^{1.6072} \cdot \left(\frac{T}{10}\right)^{0.3879} \cdot \left(\frac{w}{c}\right)^{0.4447} \cdot \left(\frac{d_c}{10}\right)^{-0.2761} \cdot K_{cl}^{1.7376} \quad (12)$$

where  $i_{corr}(t)$  is the corrosion rate ( $\mu A/cm^2$ ) at time  $t$ ,  $K_{cl}$  is the chloride concentration on the position of the reinforcement (% weight of the concrete, and limited to 0.14–0.43%),  $T$  is the temperature in degrees kelvin at the position of the reinforcement,  $RH$  is the relative humidity,  $d_c$  is the concrete cover (mm), and  $w/c$  is the water-to-cement ratio.

Kong et al. (2006)

This model is based on the study carried out by Liu and Weyers 1998. In this case, the model depends on the same parameters: chloride content, ambient temperature, and concrete resistivity.

$$\ln i_{corr}(t) = 8.617 + 0.618 \cdot \ln C_t - \frac{3034}{T} - 5 \cdot 10^{-3} \cdot \rho \quad (13)$$

where  $i_{corr}(t)$  is the corrosion rate ( $\mu A/cm^2$ ) at time  $t$ ;  $C_t$  is the chloride concentration at the reinforcement position ( $kg/m^3$ ).  $T$  is the Temperature (K) at the position of the reinforcement;  $\rho$  is the ohmic resistance of concrete (ohms), which is given by Equation (14) if the chloride concentration is less than  $3.6 kg/m^3$ , and  $\rho = 10$  if the chloride concentration is higher than  $3.6 kg/m^3$ .

$$\rho = \left[ 27.5 \cdot \left(0.35 - \frac{w}{c}\right) + 11.1 \right] \cdot (1.8 - C_t) + \left(1 - \frac{RH}{100}\right)^2 + 40 \quad (14)$$

New Empirical Model (Lu et al., 2019)

This is a recently developed corrosion rate prediction model (2019) and takes into account all factors and parameters involved in the corrosion processes of reinforcement embedded in concrete structural members. In this model, the corrosion rate is obtained by the following equation:

$$i_{corr} = \exp \left[ A + 8.617 + 0.6181 \cdot \ln(C_t) - \frac{3034}{T \cdot f(RH)} - 5 \cdot 10^{-3} \cdot \rho \right] \cdot f(t) \quad (15)$$

where  $A = -7.387$  is a constant adjustment factor,  $C_t$  chloride concentration at the reinforcement position ( $kg/m^3$ ),  $T$  is the temperature (Kelvin) at the position of the reinforcement,  $f(RH) = 2.5 + RH$  is a factor that is a function of humidity,  $RH$  is the relative humidity at the location of the structure, and  $f(t)$  is calculates as a function of the corrosion propagation time  $t_p$ , defined by Equation (15a).

$$f(t) = \frac{1}{\sqrt[3]{1 + t_p}} \quad (15a)$$



The ohmic resistance of concrete (kΩ-cm) is calculated by the method proposed in [44], whose equation is as follows:

$$\rho = \left(2.22 \cdot 10^{-4} \cdot c^2 - 0.18848 \cdot c + 48.3516\right) \cdot K_{w/b} \cdot K_{cl} \cdot K_t \cdot K_{ma} \cdot K_{pe} \tag{16}$$

where  $c$  represents the gelled material in concrete (kg/m<sup>3</sup>) and  $K_{w/b}$ ,  $K_{cl}$ ,  $K_t$ ,  $K_{ma}$ ,  $K_{pe}$  are the correction factors of the water-to-cement ratio ( $w/b$ ), chloride content, ambient temperature, mineral admixture, and external environment on the concrete resistivity, respectively, which are given by the following equations:

$$K_{w/b} = 20.895 \cdot \left(\frac{w}{b}\right)^2 - 19.551 \cdot \left(\frac{w}{b}\right) + 5.4774 \tag{16a}$$

$$K_{cl} = 607480 \cdot C_t^2 - 2242.3 \cdot C_t + 2.9926 \tag{16b}$$

$$K_T = -0.0133 \cdot T + 4.8945 \tag{16c}$$

$$K_{ma} = 1 \tag{16d}$$

where  $w/b$  is the water-to-cement ratio,  $C_t$  is the chloride content at the reinforcement position (kg/m<sup>3</sup>), and  $T$  is the temperature at the position of the reinforcement (Kelvin). For Portland cement concretes, the value used for  $K_{ma}$  shall be equal to 1. Finally,  $K_{pe}$  value shall be adopted depending on how the structure is affected by sea level.  $K_{pe}$  shall have a value equal to 1 for the atmospheric zones, a value of 0.88 for the splash zone, and 0.67 for the tidal zone [35].

The correction coefficients introduced by this new model:  $K_{w/b}$ ,  $K_{cl}$ ,  $K_t$ ,  $K_{ma}$ ,  $K_{pe}$  are quite easy to obtain, with the exception of the  $K_{ma}$  coefficient. Its value depends on the chloride concentration, the type of concrete and its additives, and the mineral mix of gelled material (kg/m<sup>3</sup>), the last two being very complex to calculate in practice. Based on the above, it has been decided to use Equation (14) to obtain the ohmic resistance of concrete, as it is less complicated.

### 3. Case Study Description

The following paragraphs provide an overview of the selected case studies in which the methodology and the corrosion prediction models stated in the previous section will be applied. The parameters to be used in the calculation of the corrosion rate and the initiation period, and how they have been obtained from the case studies, are described.

#### 3.1. Selection of Case Studies

A compilation of durability study reports, technical notes and structural repair projects has been carried out. All the documents analysed were provided by the Technical Institute of Materials and Constructions (INTEMAC). A total of 22 structures were studied from which 32 case studies were obtained. Some real images taken from these reports are shown in Figure 4. In most cases, the documentation from which the data were extracted consisted of technical notes, durability reports, and repair projects, among others. The fact that the number of case studies (32) is greater than the number of structures analysed (22) is because several case studies have been taken from a single structure, for example in the case of large structures such as viaducts or piers, several study areas with corrosion problems have been deemed appropriate to be part of the case studies.

It should be noted that the majority of the documentation corresponds to durability studies of reinforced concrete structures, as well as a short number of repair projects of prestressed concrete structures, in particular five case studies. The main descriptive data of the selected case studies are shown in Table 1. All the structures studied are privately owned and managed, thus for reasons of confidentiality no further details can be provided. A total of five different types of structure have been studied: one (1) concrete lighthouse, four (4) viaducts, one (1) bridge, two (2) piers, and one (1) quay.

**Table 1.** General data on the structures selected for the case study.

	Structure Typology	Location	Material	Construction Year <sup>1</sup>	Study Year <sup>2</sup>	Structural Element <sup>3</sup>
1	Concrete lighthouse	Canary Islands, Spain	Reinforced concrete	1976	2014	Main structure
2	Viaduct 1	Castilla-León, Spain	Prestressed concrete	1972	2007	Beam
3			Reinforced concrete			Pile 2
4			Reinforced concrete			Pile 3
5			Reinforced concrete			Pile 6
6	Bridge 1	Catalonia, Spain	Reinforced concrete	1974	2019	Beam
7	Viaduct 2	Castilla-León, Spain	Post-tensioned concrete	1972	2007	Beam
8			Reinforced concrete			Beam
9			Reinforced concrete			Pile 3
10			Reinforced concrete			Pile 6
11			Post-tensioned concrete			Beam
12	Reinforced concrete	Pile 5				
13	Pier 1	Vizcaya, Spain	Reinforced concrete	1949	2012	Beam 15
14			Reinforced concrete			Pile 22
15			Reinforced concrete			Beam 24
16			Reinforced concrete			Pile 26
17			Reinforced concrete			Beam 28
18	Quay 1	Tarragona, Spain	Reinforced concrete	1998	2016	Beam C-1
19			Reinforced concrete			Beam C-2
20			Reinforced concrete			Beam C-3
21	Pier 2	Canary Islands, Spain	Reinforced concrete	1977	2014	Beam 1
22			Reinforced concrete			Beam 2
23			Reinforced concrete			Beam 3
24			Prestressed concrete			Beam 4
25	Viaduct 3	Murcia, Spain	Reinforced concrete	1991	2014	Pile 9
26			Reinforced concrete			Pile 20
27			Reinforced concrete			Beam 6
28			Reinforced concrete			Beam 12

Table 1. Cont.

	Structure Typology	Location	Material	Construction Year <sup>1</sup>	Study Year <sup>2</sup>	Structural Element <sup>3</sup>
29	Viaduct 4	Ciudad Real, Spain	Reinforced concrete	1980	2016	Pile 8
30			Reinforced concrete			Pile 11
31			Reinforced concrete			Beam 7
32			Prestressed concrete			Beam 7

<sup>(1)</sup> Year in which the structure was first commissioned. <sup>(2)</sup> Year in which the durability study of the structure was carried out, and whose information has been collected and used for this study. <sup>(3)</sup> This is the structural element analyzed in the corresponding structure.

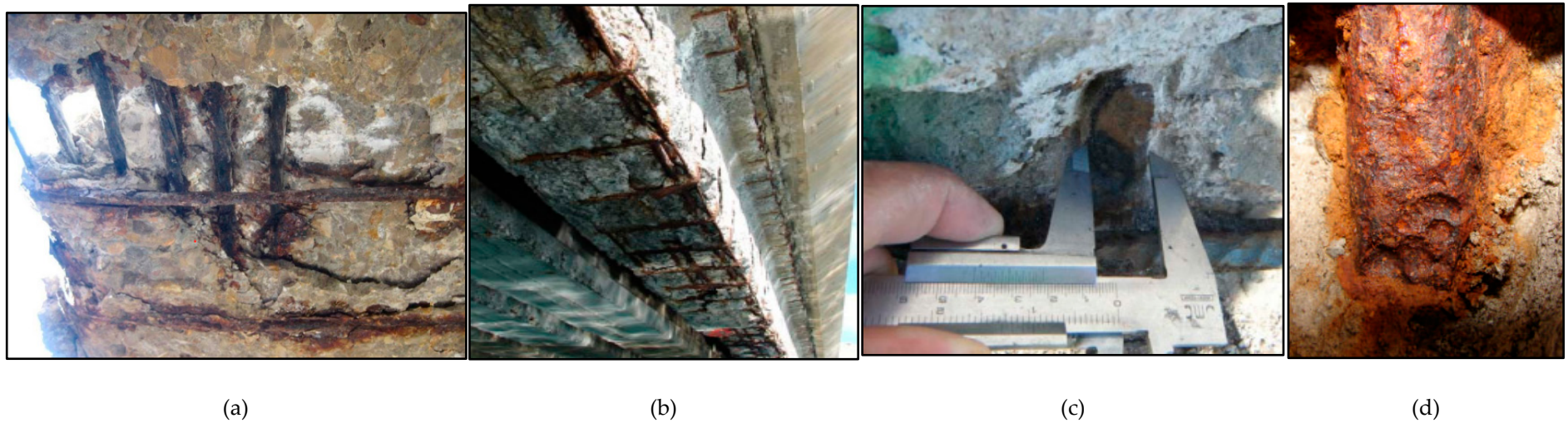


Figure 4. Structures with severe reinforcement corrosion problems. Photos obtained from the available documentation of some of the case studies (Source: Technical Institute of Materials and Constructions (INTEMAC); different dates). (a) Viaduct 4–Beam 7, (b) Pier 2–Beam 1, (c) Viaduct 3–Pile 20, and (d) Viaduct 2.

As explained above, during the application of the prediction models to the case studies, some parameters are necessary to allow the application of the different formulations involved. In order to make it easier, to identify the parameters in the documentation of each case study, the parameters are classified into two main groups

- **Concrete-dependent:** chloride concentration at reinforcement position, w/c ratio, concrete cover, and compressive strength of concrete.
- **Exposure environment of the structure:** temperature and relative humidity.

In the following sections, a brief description of the parameters is given, explaining how they have been obtained in each case study.

### 3.2. Model Parameters

#### 3.2.1. Concrete-Dependent Parameters

The chloride concentration in the position of the reinforcement is one of the key parameters and necessary in all proposed corrosion rate models. The most commonly used tool to obtain this data is to carry out chloride concentration profiles. For this purpose, test data indicating the chloride concentration at certain depths of concrete samples have been extracted from the documentation (see Table 2 of each case study). In all cases, the chloride profiles have been graphically represented (see Figure 5) in order to clearly define the chloride concentration at different depths. The chloride concentration at the position of the reinforcement, and the chloride concentration on the outer surface of the structure are required, as they are needed to calculate the corrosion rate and the initiation period through the proposed models.

**Table 2.** Compilation based on chloride concentration data in the position of pile reinforcement of Viaduct 3 (% weight of cement). (Data source: Technical Institute of Materials and Constructions (INTEMAC); May 2014).

Structural Elements	Sample Designation and Location	Chloride Content (%) at Each Depth (mm)		
		0–15	20–35	40–55
VIADUCT PILES	T-32 Pile 2	0.08	0.08	0.08
	T-33 Pile 2	0.49	0.20	0.14
	T-34 Pile 3	0.57	0.39	0.26
	T-35 Pile 3	2.20	1.93	0.38
	T-41 Pile 3	1.65	0.46	0.41
	T-23 Pile 2	0.62	0.42	0.23
	T-38 Pile 2	3.05	2.82	0.70
	T-39 Pile 1	1.99	1.70	0.57

Another important parameter is the w/c ratio. It is a very difficult parameter to obtain in existing structures if there is no available data and requires specific laboratory tests that are not usually carried out as part of the scope in durability studies. When concrete is exposed to chloride attack, it is necessary to guarantee a low permeability of the concrete in order to prevent the advance of chlorides [45]. A low w/c ratio guarantees higher permeability of the concrete, although it makes it less workable on site. Based on the above, we can say that porosity is directly related to the w/c ration of the concrete, as a low-porosity concrete will ensure a certain degree of low permeability. To obtain the w/c ratio of the case studies from available data, the following considerations have been made:

- Porosities between 12–14%, a w/c ratio of 0.45 to 0.50 is established.
- Porosities between 14–16%, a w/c ratio of 0.55 to 0.60 is established, although the latter value (0.60) can lead to even somewhat higher porosity values.

In addition to the above, the minimum  $w/c$  ratio requirements demanded by the regulations in force closest to the construction of the structures studied have been consulted in references [46,47].

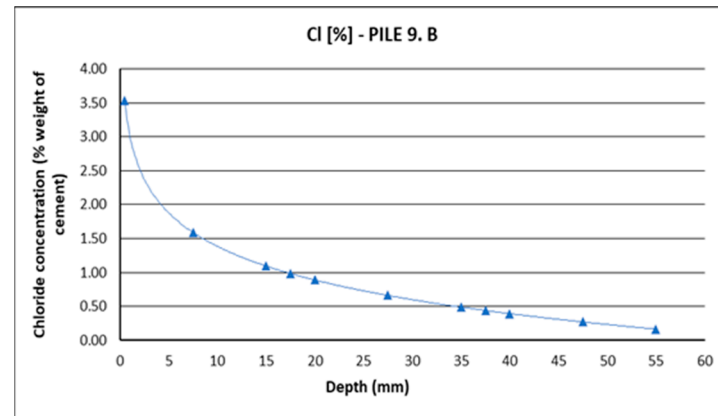


**Figure 5.** Chloride profile showing the chloride concentration as a function of depth in the test sample.

Another key parameter is the concrete cover, measured in millimetres (mm). The thickness of the concrete cover is the protection of the reinforcement against the penetration of aggressive agents such as chlorides and others and is a decisive parameter which directly conditions the corrosion initiation period. Typically, concrete cover depth is obtained by probing the study area. In this case, the concrete cover has been obtained from the documentation of each case study.

Finally, for the model proposed by Vu and Stewart (2000), the concrete compressive strength ( $f_{ck}$ ) data is required. This parameter is obtained from the results of simple compression tests on concrete specimens. It is very common to carry out this type of tests as part of the materials characterisation campaign in durability studies of structures, thus it was easy to obtain this parameter from the documentation of each case study.

### 3.2.2. Parameters Depending on the Exposure Environment

The two parameters that depend on the exposure environment in the location of structures are temperature and the relative humidity

Firstly, two important aspects should be highlighted with regard to the parameter of temperature. On the one hand, it is a complex task to measure the temperature at the exact position of the reinforcement as required by some corrosion rate models, thus the value of the average annual temperature where the structure is located has been taken, since the thermal variations in the depth of the concrete up to the position of the reinforcement are minimal according to [42]. As the structures of the 32 cases are located on Spanish territory, data from the State Meteorological Agency [48] have been used to obtain the mean temperature data. As in the corrosion rate models, the unit of temperature is in degrees kelvin (K), it has been necessary to convert the unit from degrees Celsius ( $^{\circ}\text{C}$ ) to degrees kelvin (K), as the data from the meteorological agency are in degrees Celsius.

The relative humidity parameter is required in several of the proposed models. Average annual relative humidity values have been used for the area around the structure under study. In the same way, these data have been provided by the State Meteorological Agency depending on the location of the structure.

## 4. Results

Formula application and validity are here presented together with the results obtained for the different case studies, which are shown below according to the methodology and different equations previously exposed.

The section is divided into two parts, where the results obtained from the propagation time in each case study are shown first. The second part of the results shows the calculated diameter loss in each case study with the corrosion rate of each model.

#### 4.1. Propagation Period

The propagation period is an essential parameter to calculate the loss of reinforcement diameter (see Equation (2)). In addition, it is a parameter required by the models of Vu and Stewart (2000) and Li (2004) to calculate the corrosion rate. This section explains how to calculate the propagation period with the help of an example.

To obtain the propagation period, the corrosion initiation period is first calculated using the chloride diffusion model proposed by the Spanish code on structural concrete (EHE-08) [38], as explained previously in the methodology. Table 3 shows the calculation of the initiation period for the case study of pier 9 of viaduct 3 using the indications of the structural code and Equations (3)–(5) and all the parameters necessary for its calculation.

**Table 3.** Calculation of the corrosion initiation period. Example: Pier 9, Viaduct 3.

Calculation of the Initiation Period (Years)		
Parameter	Source	Data
Concrete Cover	Structure documentation	40 mm
Service life of the structure	Structure documentation	23 years
Cement type	Structure documentation	CEM I
Porosity	Structure documentation	13.4%
w/c ratio	Based on porosity	0.5
$D(t_0)$	Table A.9.4 (EHE-08)	$1.58 \times 10^{-11} \text{ m}^2/\text{s}$
$t_0$	Section 1.2.2.2 (EHE-08)	0.0767 years
n	Section 1.2.2.2 (EHE-08)	0.5
$C_s$ (% weight cement)	Chloride profiles	3.53
$C_{th}$ (% weight cement)	EHE-08 recommendation	0.6
$C_b$ (% weight cement)	EHE-08 recommendation	0.4
Reinforcement diameter	Structure documentation	25 mm
$K_{cl}$	(Equation (4))	13.88
Initiation period	(Equation (3))	8.30 years

The difference between the age of the structure at the time the durability study was carried out and the initiation period is the propagation period. In this case, the initiation period is 8.30 years, and the age of the structure when the study was carried out is 23 years, therefore, the propagation period is 14.7 years. Table 4 shows the propagation time results obtained for each case study.

#### 4.2. Calculation of Diameter Loss

##### 4.2.1. Liu & Weyers (1998)

The 32 case studies (5 prestressed concrete and 27 reinforced concrete) have been considered, comparing the diameter loss values in the reinforcements obtained with the corrosion rate model and the real diameter loss obtained from the documentation of each case study. Table 5 shows the results obtained.

When analyzing the results, only 4 cases (21, 22, 23, and 24 of those described in Table 2) have diameter loss values similar to the real ones. In all these cases, the section loss obtained with the model ( $P_x$ ) has always been slightly higher than the real diameter loss ( $P_r$ ), guaranteeing an average safety factor of 1.5. In the remaining 28 cases, the values obtained with the model are far from reality, not guaranteeing the necessary safety margin.

Furthermore, from the results, it has been observed that in the case of prestressed and post-tensioned concrete structures (2, 7, 11, 24, and 32) the values obtained with the corrosion rate prediction model are even further away from the reality than in the case of reinforced concrete structures.

**Table 4.** Propagation period results for each of the case studies. Calculated from the age of the structure at the time of the durability study ( $t_s$ ) and the initiation period ( $t_i$ ).

N°	$t_s$ (Years)	Initiation Period $t_i$ (Years)	Propagation Period $t_p$ (Years) = $t_s - t_i$
1	38	11.39	26.61
2	35	18.60	16.40
3	35	3.95	31.05
4	35	3.49	31.51
5	35	4.40	30.60
6	45	11.81	33.52
7	35	7.14	27.86
8	35	2.79	32.21
9	35	3.11	31.89
10	35	3.11	31.89
11	35	8.89	26.11
12	35	3.55	31.45
13	63	2.84	60.16
14	63	7.36	55.64
15	63	8.09	54.91
16	63	6.87	56.13
17	63	12.09	50.91
18	18	9.54	8.46
19	18	10.15	7.85
20	18	9.82	8.18
21	37	10.90	26.10
22	37	15.87	21.13
23	37	9.11	27.89
24	37	17.86	19.14
25	23	16.63	6.37
26	23	8.30	14.70
27	23	5.23	17.77
28	23	5.71	17.29
29	36	24.02	11.98
30	36	10.18	25.82
31	36	10.42	25.58
32	36	9.17	26.83

**Table 5.** Case studies with favourable results using the Liu & Weyers (1998) model.

N°	Real Diameter Loss $P_r$ (mm)	Diameter Loss Liu & Weyers $P_x$ (mm)-Equation (2)	Safety Factor $P_x/P_r$
21	1.20	1.493	1.24
22	0.60	0.856	1.43
23	0.60	1.788	2.98
24	0.80	1.281	1.60

#### 4.2.2. Vu and Stewart (2000)

As far as the data analysis is concerned, of the 32 cases studied, in 18 of them (56.25% of the total sample), the diameter loss value obtained using the model is greater than real diameter loss. The safety factor provided by the model for these 18 cases is approximately 2.29. Table 6 shows the results obtained.

In the 5 cases of prestressed and post-tensioned concrete structures analyzed (2, 7, 11, 24, and 32), in 4 of them the model values are far away from the real values (safety margin 0.40), while in the only case that meets the safety criteria, the result obtained from the model is four times higher than the real value.

**Table 6.** Case studies with favourable results using the Vu and Stewart (1998) model.

N°	Real Diameter Loss Pr (mm)	Diameter Loss Liu & Weyers Px (mm)-Equation (2)	Safety Factor Px/Pr
6	5.10	9.408	1.84
3	4.00	4.988	1.25
4	4.00	4.667	1.17
5	4.00	5.511	1.38
8	3.60	3.884	1.08
13	6.25	11.575	1.85
14	5.00	7.157	1.43
16	9.00	11.534	1.28
17	5.00	9.469	1.89
18	1.00	1.486	1.49
19	1.50	2.105	1.40
20	1.00	3.200	3.20
21	1.20	5.373	4.48
22	0.60	6.462	10.77
23	0.60	6.027	10.05
24	0.80	3.396	4.25
26	0.50	4.083	8.17
29	2.10	2.155	1.03

#### 4.2.3. Li (2004 a)

Undoubtedly, this model, besides being the simplest for its application to real cases, is also the one that has given the best results. Table 7 shows the results obtained, in which of the 32 cases studied, 26 of them are favorable, which means that the diameter loss obtained with the model is greater than the real diameter loss. Only six cases are unfavorable, which means that the diameter loss obtained with the model is smaller than the actual diameter loss, although with values very close to the real ones.

The safety factor obtained is 1.98 on average, which means that, in the favorable cases, the section loss value obtained by the model is twice the real value. The distribution of this average is quite homogeneous, varying between 1.73 and 2.07 in most cases. In the six unfavorable cases, the values obtained are very close to real values of diameter loss.

As for the prestressed and post-tensioned concrete structures analysed with this model, the trend changes with respect to the previous ones. Of the five prestressed cases studied, the results were favourable in three of them, while in the remaining two the results were unfavourable.

#### 4.2.4. Li (2004 b)

The section loss results obtained were not satisfactory, since of the 32 cases studied, 22 of them have been unfavourable, with diameter loss results much lower than the real ones, with a safety coefficient of 0.45. Of the 10 cases where the diameter loss value is higher than the real one, the results are not particularly encouraging, as the safety factor is very tight in some cases—1.51 on average. Table 8 shows the results obtained with this model.

Of the five prestressed and post-tensioned concrete structures cases analysed, in one of them (case number 24), favourable results have been obtained through the model, with a safety factor of 1.37. In the remaining four cases, the results obtained are one below the real values of diameter loss.

#### 4.2.5. Kong et al. (2006)

The results of this model have not been favourable. Only in case number 23, the diameter loss value calculated with the model was higher than the actual diameter loss. In this case, the diameter loss calculated with the corrosion rate of the model was 0.605 mm, while the real diameter loss in the reinforcement is 0.60 mm. These results barely guarantee a safety factor of 1.01.



**Table 7.** Case studies with favourable results using the Li (2004 a) model.

N°	Real Diameter Loss Pr (mm)	Diameter Loss Li (2004) Px (mm)-Equation (2)	Safety Factor Px/Pr
6	5.10	7.540	1.48
3	4.00	6.903	1.73
4	4.00	7.022	1.76
5	4.00	6.788	1.70
8	3.60	7.202	2.00
9	4.00	7.119	1.78
10	4.00	7.119	1.78
11	5.00	5.650	1.13
13	6.25	14.736	2.36
14	5.00	12.179	2.44
15	6.25	13.278	2.12
16	9.00	13.615	1.51
17	5.00	13.480	2.70
18	1.00	1.505	1.50
20	1.00	1.446	1.45
21	1.20	5.648	4.71
22	0.60	4.420	7.37
23	0.60	6.099	10.16
24	0.80	3.939	4.92
25	2.00	2.893	1.45
26	0.50	1.071	2.14
27	3.00	3.612	1.20
29	2.10	2.274	1.08
30	2.70	5.578	2.07
31	5.00	5.518	1.10
32	4.00	5.831	1.46

**Table 8.** Case studies with positive results using the Li (2004 b) model.

N°	Real Diameter Loss Pr (mm)	Diameter Loss Liu and Weyers Px (mm)-Equation (2)	Safety Factor Px/Pr
12	10.00	11.270	1.13
13	6.25	12.885	2.06
15	6.25	21.462	3.43
16	9.00	7.287	1.19
17	5.00	10.697	1.46
18	1.00	1.311	1.31
21	1.20	1.637	2.21
22	0.60	1.325	2.91
23	0.60	1.749	1.75
24	0.80	1.094	1.37

#### 4.2.6. New Empirical Model (Lu et al., 2019)

In the results obtained with this model, 25 of the 32 cases analysed were unfavourable. The seven cases shown in Table 9 have positive results, where the diameter loss calculated through the corrosion rate of this model has been higher than the real diameter loss. The average safety factor obtained is 1.5.

In the case of prestressed and post-tensioned concrete structures, the trend is exactly the same as in the rest of the models. All section loss values calculated with this model for this type of structure are much lower than the actual diameter loss.

**Table 9.** Case studies with favourable results using the New Empirical model (2019).

Nº	Real Diameter Loss Pr (mm)	Diameter Loss New Model Px (mm)	Safety Factor Px/Pr
18	1.00	1.118	1.12
20	1.00	1.031	1.03
21	1.20	2.199	1.83
22	0.60	1.389	2.31
23	0.60	2.558	4.26
24	0.80	1.901	2.38
26	0.50	0.571	1.14

## 5. Discussion

### 5.1. Comparison of Model Results

To compare the results presented previously, this study analysed which of the corrosion rate calculation models has the highest number of cases where the diameter loss calculated with the proposed methodology is higher than the actual diameter loss.

The graph in Figure 6 shows the distribution between the calculated diameter loss with each of the models and the actual observed diameter loss. When the difference between the two is greater than zero, it means that the value calculated through the model is greater than the actual observed diameter loss.

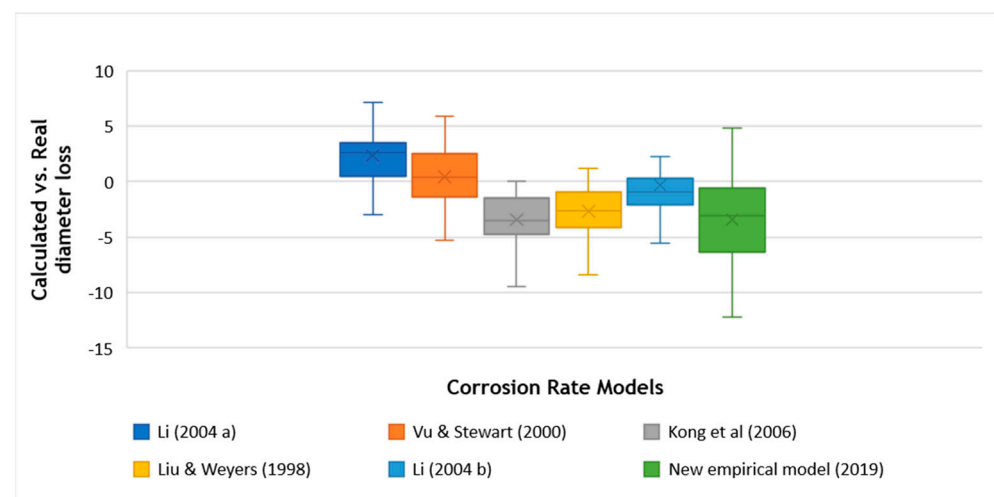


**Figure 6.** Distribution of estimated vs. real diameter loss in the study cases with different corrosion rate models.

It can be seen that only the Li (2004 a) model has the best performance, as it is the only one with a positive mean of the deviations, and this deviation is positive for more than 75% of the cases studied. In the Vu and Stewart (2000) model, the mean is practically zero and the model has the same probability of hitting and missing, as the median is also at zero.

In the rest of the models, the mean is clearly negative, and as can be seen in more than 75% of the cases, the diameter loss calculations with the model would be wrong.

Therefore, the results of the combination of the chloride diffusion model (EHE-08) for the calculation of the initiation period and the corrosion rate calculation model Li (2004 a) have given the most satisfactory results. In addition to the importance of efficiency in as many cases as possible, ensuring optimal safety margins between the calculated results and reality is also very important.

Figure 7 shows the safety factors obtained for each case study. In 26 of the 32 cases studied, the safety factors are at least greater than one (orange line), and practically all the values are homogeneously between one and two (green line). There are six cases where the diameter loss calculated with the model is less than the actual diameter loss of the

reinforcement (red color bar). Only in four of the cases are the safety factors significantly higher than two. This means that in addition to the model having a high probability of success, the safety factors obtained are very reasonable, and similar to the safety coefficients factors used in the design of concrete structures.

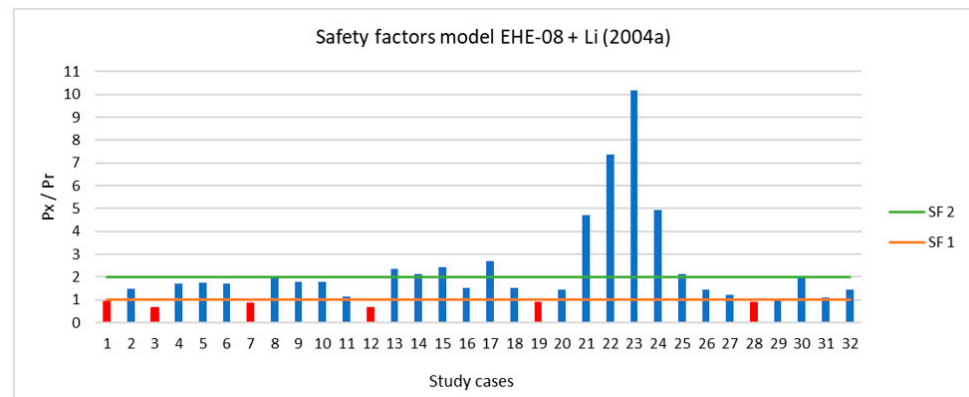


Figure 7. Safety factors obtained for each case study by applying the EHE-08 + Li (2004) model.

In reference to prestressed or post-tensioned cases, none of the models have been very successful. Table 10 shows the corrosion rate models and the number of cases where the result was positive. As can be seen, there are a limited number of cases of prestressed or post-tensioned concrete, where the value of the diameter loss calculated with the models is higher than the actual diameter loss. The best performer is again the model of Li (2004 a), with three cases with favourable results. In the case of the model of Kong et al. (2006), none of the five cases studied is favourable. These poor model results in prestressed or post-tensioned concrete structures may be due to stress corrosion cracking phenomena, which are different from conventional corrosion processes [49,50].

Table 10. Corrosion rate models and number of cases of prestressed and post-tensioned concrete structures with favourable results.

Corrosion Rate Model	Number of Positive Cases	Study Case
Liu & Weyers (1998)	1	24
Kong et al. (2006)	0	0
Vu & Stewart (2000)	1	24
Li (2004 a)	3	11, 24, 32
Li (2004 b)	1	24
New Empirical Model (Lu et al., 2019)	1	24

After analysing the results presented in the previous section and comparing the different corrosion rate models proposed, it can be seen that the model with the best estimates of diameter loss in the 32 cases studied was the corrosion rate model proposed by Li (2004 a). These good results are also related to a good combination between the model of Li (2004 a), which represents the corrosion propagation phase, and the chloride diffusion model of the (EHE-08), which has allowed the characterisation of the corrosion initiation time. In combination, these two proposed models have made it possible to obtain, with simple calculations, an estimated value of diameter loss in the reinforcement that is very close to reality in a representative sample of real cases of reinforced and prestressed concrete structures affected by corrosion.

### 5.2. Potential Applications

Using the proposed methodology and the validated corrosion prediction models, it is possible to know with a high level of confidence the loss of diameter suffered by a reinforcement affected by corrosion as a function of propagation time and corrosion rate

and therefore create a tool to know how the resistance capacity of any structural element affected by corrosion problems varies during lifetime. This has great potential in the field of maintenance of offshore structures such as concrete foundations and is a fundamental tool for any operator to plan appropriate maintenance strategies and to optimise human and material resources while guaranteeing structural safety during lifetime.

For this purpose, and based on the methodology proposed in the previous chapter, spreadsheets have been created as a tool to obtain the coefficient of resistant variation  $K$ , which indicates a measure of loss of structural safety, as indicated in the Equation (17).

$$K = \frac{R_a}{R_n} \tag{17}$$

where  $R_a$  is the altered resistant capacity (affected by the diameter loss as a result of corrosion) and  $R_n$  is the nominal resistance capacity.

When this coefficient is close to 1, the altered resistant capacity of the element is close to the nominal resistant capacity. As the value of the coefficient moves away below the unit value, the altered resistant capacity of the element is less than the nominal resistant capacity, which can be a risk to safety and security. In this case, a limit shall be established that, for those values close to  $K = 0.85$ , structural strengthening or other actions shall be considered to ensure the proper functioning of the element and the minimum necessary safety conditions.

Figure 8 shows an example for a reinforced concrete element working in simple bending and affected by corrosion problems in its principal reinforcement. This tool is equally applicable to other structural elements in compression or shear. On the x-axis is the age of the structure, and on the y-axis is the safety loss coefficient ( $K$ ) expressed as a percentage. As can be seen, at approximately 27 years of age, the main bending reinforcement of the structure would have lost sufficient section to cause a loss of resistance capacity of 15% of the nominal resistance capacity.



**Figure 8.** Estimation of the loss of strength capacity over its service life of a structural element working on single flexure with corrosion problems in its main reinforcement.

This means that, under the criterion of considering actions once there has been a 15% loss of strength of the element, at 27 years of age of the structure, it would be necessary to carry out a repair or reinforcement action of the structural element. By the time the structure is 61 years old, it will have lost approximately 60% of its load-bearing capacity, indicating an imminent risk of collapse.

With this analytical data, it is easier to plan and optimise the maintenance of the structures, especially when it comes to offshore wind turbine foundations that are located

in marine environments that are very difficult to access, and where any maintenance activity is very costly for the project.

## 6. Conclusions

Finally, the main conclusions of this paper are set out in the following points:

- In more than 75% of the 32 case studies, the application of the chloride diffusion model of the EHE-08 and the corrosion rate calculation model of Li (2004 a) has resulted in similar diameter loss values when compared to real reinforced and prestressed concrete structures that have been affected by active corrosion processes. The calculated diameter loss results promise reasonable safety coefficients, with a minimum value of 1.73, and the average safety factor of 1.98. This means that the diameter loss value calculated through the models is twice as high as the actual diameter loss.
- The combination of the EHE-08 diffusion model and the Vu and Stewart (2000) corrosion rate calculation model is the next best performer in diameter loss. In this case, the median is zero, which means that the combination of models has approximately the same probability of success as failure in a case study.
- The combination of the EHE-08 chloride diffusion model and the other corrosion rate calculation models: Liu and Weyers (1998), Li (2004 b), Kong et al. (2006), and New Empirical Model (Lu et al., 2019) has not obtained satisfactory results. The calculated reinforcement diameter losses were generally much lower in practically all cases, with the combination with the model of Kong et al. (2006) giving the worst results.
- The application of the EHE-08 diffusion model with none of the corrosion rate calculation models proposed, has proved satisfactory results in the case studies of prestressed and post-tensioned concrete structures analyzed as part of the whole sample. Again, the model of Li (2004 a), together with the chloride diffusion model of the EHE-08, gave the best results in this aspect.
- A tool for rapidly estimating the section loss of reinforcement in offshore concrete structural elements as a function of time provides offshore wind farm operators with a cost-effective approach for planning their maintenance strategies and the optimisation of material costs and human resources. This is essential, considering the exponential expansion of O&M costs, and where reinforced concrete will continue to be represented.

**Author Contributions:** Conceptualization, M.D.E., R.R.R. and K.V.; methodology, M.D.E., R.R.R. and K.V.; validation, M.D.E., R.R.R. and K.V.; formal analysis, M.D.E., R.R.R. and K.V.; investigation, K.V.; writing—original draft preparation, M.D.E., R.R.R. and K.V.; writing—review and editing, M.D.E., R.R.R. and K.V.; supervision, R.R.R. and M.D.E. All authors have read and agreed to the published version of the manuscript.

**Funding:** Not applicable.

**Institutional Review Board Statement:** Not applicable.

**Informed Consent Statement:** Not applicable.

**Data Availability Statement:** Data available on request due to privacy restrictions. The data presented in this study are available on request from the corresponding author. The data are not publicly available due to confidential reasons.

**Acknowledgments:** K.V.; R.R.R. and M.D.E. are very grateful to the Technical Institute of Materials and Constructions (INTEMAC) for providing us with the case studies and all the documentation necessary to carry out this research work.

**Conflicts of Interest:** The authors declare no conflict of interest.

## References

1. Ramírez, L.; Brindley, G. Offshore Wind Energy: 2021 Mid-Year Statistics. 2021. Available online: [Windeurope.org](https://windeurope.org) (accessed on 10 November 2021).
2. Lee, J.; Zhao, F. Global Offshore Wind Report 2021. 2021. Available online: <http://www.gwec.net/global-figures/wind-energy-global-status/> (accessed on 10 November 2021).
3. International Renewable Energy Agency. Renewable Energy Statistics 2021. 2021. Available online: <https://www.irena.org/publications/2021/March/Renewable-Capacity-Statistics-2021> (accessed on 10 November 2021).
4. European Union. Regulation (EU) 2021/1119 of the European Parliament and of the Council of 30 June 2021 Establishing the Framework for Achieving Climate Neutrality and Amending Regulations (EC) No 401/2009 and (EU) 2018/1999 ('European Climate Law'). 2021. Available online: <https://eur-lex.europa.eu/legal-content/EN/TXT/PDF/?uri=CELEX:52019DC0640&from=EN> (accessed on 10 November 2021).
5. European Commission. In-Depth Analysis in Support of the Commission Communication Com (2018) 773: A Clean Planet for all A European Long-Term Strategic Vision for a Prosperous, Modern, Competitive and Table of Contents. 2018. Available online: [https://knowledge4policy.ec.europa.eu/publication/depth-analysis-support-com2018-773-clean-planet-all-european-strategic-long-term-vision\\_en](https://knowledge4policy.ec.europa.eu/publication/depth-analysis-support-com2018-773-clean-planet-all-european-strategic-long-term-vision_en) (accessed on 10 November 2021).
6. European Commission. Guidance Document on Wind Energy Developments and EU Nature Legislation. 2020. Available online: [https://ec.europa.eu/environment/nature/natura2000/management/docs/wind\\_farms\\_en.pdf](https://ec.europa.eu/environment/nature/natura2000/management/docs/wind_farms_en.pdf) (accessed on 15 October 2021).
7. Fraile, I.K.D.; Vandenberghe, A.; Klonari, V.; Ramirez, L.; Pineda, I.; Tardieu, P.; Malvault, B. Getting Fit for 55 and Set for 2050. 2021. Available online: <https://windeurope.org/intelligence-platform/product/getting-fit-for-55-and-set-for-2050/#> (accessed on 10 November 2021).
8. Johnston, B.; Foley, A.; Doran, J.; Littler, T. Levelised cost of energy, A challenge for offshore wind. *Renew. Energy* **2020**, *160*, 876–885. [[CrossRef](#)]
9. Mone, C.; Stehly, T.; Maples, B.; Settle, E. 2017 Cost of Wind Energy Review. 2017. Available online: <https://www.nrel.gov/docs/fy18osti/72167.pdf> (accessed on 15 March 2021).
10. Crabtree, C.J.; Zappalá, D.; Hogg, S.I. Wind energy: UK experiences and offshore operational challenges. *Proc. Inst. Mech. Eng. Part A J. Power Energy* **2015**, *229*, 727–746. [[CrossRef](#)]
11. BVG. Associates. Value Breakdown for The Offshore Wind Sector. 2010. Available online: [https://www.gov.uk/government/uploads/system/uploads/attachment\\_data/file/48171/2806-value-breakdown-offshore-wind-sector.pdf](https://www.gov.uk/government/uploads/system/uploads/attachment_data/file/48171/2806-value-breakdown-offshore-wind-sector.pdf) (accessed on 12 April 2021).
12. Miedema, R. Offshore Wind Energy Operations & Maintenance Analysis. Research Thesis, Hogeschool Van Amsterdam, Amsterdam, The Netherlands. 2012. Available online: [http://sciencecentre.amccentre.nl/studies/Thesis\\_Robert\\_Miedema.pdf](http://sciencecentre.amccentre.nl/studies/Thesis_Robert_Miedema.pdf) (accessed on 15 March 2021).
13. Wu, X.; Hu, Y.; Li, Y.; Yang, J.; Duan, L.; Wang, T.; Adcock, T.; Jiang, Z.; Gao, Z.; Lin, Z.; et al. Foundations of offshore wind turbines: A review. *Renew. Sustain. Energy Rev.* **2018**, *104*, 379–393. [[CrossRef](#)]
14. Sánchez, S.; López-Gutiérrez, J.S.; Negro, V.; Esteban, M.D. Foundations in offshore wind farms: Evolution, characteristics and range of use. Analysis of main dimensional parameters in monopile foundations. *J. Mar. Sci. Eng.* **2019**, *7*, 441. [[CrossRef](#)]
15. Esteban, M.D.; Matutano, C. Offshore Wind Foundation Design: Some Key Issues. *J. Energy Resour. Technol.* **2015**, *137*, 1–6. [[CrossRef](#)]
16. Fernández, R.P.; Pardob, M.L. Offshore concrete structures. *Ocean Eng.* **2013**, *58*, 304–316. [[CrossRef](#)]
17. Esteban, M.D.; López-Gutiérrez, J.-S.; Negro, V. Gravity-Based Foundations in the Offshore Wind Sector. *J. Mar. Sci. Eng.* **2019**, *7*, 64. [[CrossRef](#)]
18. Trust, T.C. Offshore Wind Industry Review of GBS. 2015. Available online: [https://prod-drupal-files.storage.googleapis.com/documents/resource/public/Offshore\\_wind\\_industry\\_review\\_of\\_Gravity\\_Based\\_Structures\\_REPORT.pdf](https://prod-drupal-files.storage.googleapis.com/documents/resource/public/Offshore_wind_industry_review_of_Gravity_Based_Structures_REPORT.pdf) (accessed on 20 December 2021).
19. Esteban, M.D.; Couñago, B.; López-gutiérrez, J.S.; Negro, V.; Vellisco, F. Gravity based support structures for offshore wind turbine generators: Review of the installation process. *Ocean Eng.* **2015**, *110*, 281–291. [[CrossRef](#)]
20. Rodrigues, S.; Restrepo, C.; Kontos, E.; Pinto, R.T.; Bauer, P. Trends of offshore wind projects. *Renew. Sustain. Energy Rev.* **2015**, *49*, 1114–1135. [[CrossRef](#)]
21. WindEurope—The Voice of the Wind Energy Industry. Available online: <https://windeurope.org/> (accessed on 16 December 2021).
22. Mathern, A.; von der Haar, C.; Marx, S. Concrete support structures for offshore wind turbines: Current status, challenges, and future trends. *Energies* **2021**, *14*, 1995. [[CrossRef](#)]
23. ELISA—Elican Project. Esteyco. Available online: <https://www.esteyco.com/proyectos/elisa-elican-project/> (accessed on 16 December 2021).
24. James, R.; Ros, M.C. Floating Offshore Wind: Market and Technology Review. *Carbon Trust* **2015**, *439*. [[CrossRef](#)]
25. International Renewable Energy Agency (IRENA). Innovation Outlook: Offshore Wind. Available online: <https://www.irena.org/publications/2016/oct/innovation-outlook-offshore-wind> (accessed on 12 December 2021).
26. DNV GL. DNVGL-ST-0126: Support Structures for Wind Turbines. 2018. Available online: <https://rules.dnvgl.com/docs/pdf/DNVGL/ST/2018-07/DNVGL-ST-0126.pdf> (accessed on 15 May 2021).
27. ACI Committee 222. Protection of Metals in Concrete Against Corrosion. In *ACI 222R-01*; ACI: Farmington Hills, MI, USA, 2001; pp. 1–41.

28. EC Innovation Programme; Andrade, C.; Izquierdo, D. A Validated Users Manual for Assessing the Residual Service Life of Concrete Structures. Madrid. 2001. Available online: [https://www.ietcc.csic.es/wp-content/uploads/1989/02/manual\\_contecvet\\_ingles.pdf](https://www.ietcc.csic.es/wp-content/uploads/1989/02/manual_contecvet_ingles.pdf) (accessed on 20 October 2021).
29. Feliu, S.; Andrade, C. Manual: Inspección de Obras Dañadas por Corrosión de Armaduras. In *Acor*; IETCC: Madrid, Spain, 1989; pp. 1–122. [CrossRef]
30. Odriozola, M.Á.B. Corrosión de las Armaduras del Hormigón Armado en Ambiente Marino: Zona de Carrera de Mareas y Zona Sumergida. Ph.D. Thesis, Universidad Politécnica de Madrid, Madrid, Spain, 2007.
31. Pruckner, F. Diagnosis and Protection of Corroding Steel in Concrete. Ph.D. Thesis, Norwegian University of Science and Technology Faculty of Engineering Science and Technology Department of Structural Engineering, Trondheim, Norway, November 2002.
32. Ciolko, A. *Nondestructive Methods for Condition Evaluation of Prestressing Steel Strands Nondestructive Methods for Condition Evaluation of Prestressing Steel Strands in Concrete Bridges Final Report Phase I: Technology Review*; Prepared for National Cooperative Highway Research Program; no. July 2015; NCHRP: Washington, DC, USA, 1999.
33. Liu, L.; Fu, Y.; Ma, S.; Huang, L.; Wei, S.; Pang, L. Optimal scheduling strategy of O&M task for OWF. *IET Renew. Power Gener.* **2019**, *13*, 2580–2586. [CrossRef]
34. Shafiee, M. Maintenance logistics organization for offshore wind energy: Current progress and future perspectives. *Renew. Energy* **2015**, *77*, 182–193. [CrossRef]
35. Lu, Z.H.; Lun, P.Y.; Li, W.; Luo, Z.; Li, Y.; Liu, P. Empirical model of corrosion rate for steel reinforced concrete structures in chloride-laden environments. *Adv. Struct. Eng.* **2019**, *22*, 223–239. [CrossRef]
36. Tutti, K. Corrosion of Steel in Concrete. Swedish Cement and Concrete Research Institute. 1982. Available online: <http://www.cbi.se/viewNavMenu.do?menuID=317&oid=857> (accessed on 15 May 2021).
37. García, S.F. Corrosión De Armaduras En El Hormigón Armado En Ambiente Marino Aéreo. Ph.D. Thesis, Universidad Politécnica de Madrid, Madrid, Spain, 2016. Available online: [https://oa.upm.es/39374/1/Susana\\_Fernandez\\_Garcia.pdf](https://oa.upm.es/39374/1/Susana_Fernandez_Garcia.pdf) (accessed on 16 April 2021).
38. Comisión Permanente del Hormigón. Instrucción de Hormigón Estructural (EHE-2008). 2011. Available online: <http://www.ponderosa.es/docs/Norma-EHE-08.pdf> (accessed on 20 December 2021).
39. Helland, S.; Aarstein, R.; Maage, M. In-field performance of North Sea offshore platforms with regard to chloride resistance. *Struct. Concr.* **2010**, *11*, 15–24. [CrossRef]
40. Markeset, G.; Myrdal, R. Modelling of Reinforcement Corrosion in Concrete-State of the Art. 2008. Available online: <http://smartpipe.com/upload/Byggforsk/Publikasjoner/coin-no7.pdf> (accessed on 22 February 2021).
41. Bertolini, L.; Elsener, B.; Pedferri, P.; Redalli, E.; Polder, R. *Corrosion of Steel in Concrete. Prevention, Diagnosis, Repair*; Wiley: Hoboken, NJ, USA, 2013.
42. Zhang, D.; Zeng, Y.; Fang, M.; Jin, W. Service life prediction of precast concrete structures exposed to chloride environment. *Adv. Civ. Eng.* **2019**, *2019*, 3216328. [CrossRef]
43. Liu, Y. Modeling time-to-corrosion cracking in chloride contaminated reinforced concrete structures. *ACI Mater. J.* **1999**, *96*, 611–613. Available online: <https://trid.trb.org/view/514367> (accessed on 15 April 2021).
44. Yu, B.; Yang, L.; Wu, M.; Li, B. Practical model for predicting corrosion rate of steel reinforcement in concrete structures. *Constr. Build. Mater.* **2014**, *54*, 385–401. [CrossRef]
45. Gjorv, O.E. *Durability Design of Concrete Structures in Severe Environments*; Routledge: Abingdon-on-Thames, UK, 2014.
46. Ministerio de Obras Públicas. *Instrucción para el Proyecto y la Ejecución de Obras de Hormigón en Masa o Armado (EH-88)*; Ministerio de Obras Públicas: Madrid, Spain, 1988.
47. Ministerio de Obras Públicas. *Instrucción para el Proyecto y Ejecución de Obras de Hormigón*, 1st ed.; Ministerio de Obras Públicas: Santander, Spain, 1939; Volume 1.
48. Agencia Estatal de Meteorología—AEMET. Gobierno de España. Available online: <http://www.aemet.es/es/portada> (accessed on 18 December 2021).
49. Hurtado, M.A. Corrosion Bajo Tension De Alambre de Acero Pretensado en Medios Neutros con HCO<sub>3</sub> y Alcalinos con SO<sub>4</sub>. Ph.D. Thesis, Universidad Complutense Madrid, Madrid, Spain, 1993.
50. Khalifeh, A. Stress Corrosion Cracking Damages. In *Failure Analysis*; InTech Open: London, UK, 2019. [CrossRef]